African Journal of Advanced Pure and Applied Sciences (AJAPAS)
Online ISSN: 2957-644X
Volume 5, Issue 4, 2026
Page No: 9-22
Website: https://aaasjournals.com/index.php/ajapas/index
ISI 2025: 1.126 SJIFactor 2024: 6.752 معامل التأثير العربي 2025: 1.65

In Silico Docking and ADMET Profiling of Cyclopentane-Based Enaminones as Candidate PARP1 Inhibitors

Abdalhamid Alarafi [1 *], Mohammed A. Alajilani [2], Haneen A. Awali [3], Raghad Abdulfatah Mohammed [4]
[1, 2, 4] Department of Chemistry, Faculty of Arts and Sciences, University of Benghazi, Al-Abyar, Libya
[3] Libyan Center for Studies and Research of Environmental Science and Technology, Sabartha, Libya

دراسة محاكاة الارتباط الجزيئي وتحليل خصائص الامتصاص والتوزيع والاستقلاب والإخراج والسمية لمركبات الإينامينون المشتقة من السيكلوبنتان كمرشحات لتثبيط إنزيم *PARP1*

عبدالحميد العرفي [1*]، محمد الجيلاني [2]، حنين والي [3]، رغد عبد الفتاح [4]
[4, 2, 1] قسم الكيمياء، كلية العلوم، جامعة بنغازي، الأبيار، ليبيا
[3] المركز الليبي لدراسات وبحوث علوم وتكنولوجيا البيئة، صبراتة، ليبيا

[*]Corresponding author: abdalhamid.abdallah@uob.edu.ly

Received: July 15, 2026	Accepted: September 26, 2026	Published: October 05, 2026

Abstract:
Poly(ADP-ribose) polymerase 1 (PARP1) represents a significant therapeutic target in cancer treatment focused on DNA repair; yet, cyclopentane-derived enaminones have not been extensively investigated as chemotypes that bind to PARP1. In this research, ten previously created cyclopentane-derived enaminone compounds (1A–5A and 1B–5B) were assessed through structure-based molecular docking against the catalytic domain of human PARP1 (PDB ID: 7KK4), followed by thorough in silico evaluations of pharmacokinetics, drug-likeness, and toxicity. The docking protocol was confirmed through re-docking the co-crystallized inhibitor olaparib, resulting in an RMSD of 1.183 Å. The studied derivatives showed docking S-scores between −6.234 and −7.972 kcal/mol, with compounds 1B (−7.972 kcal/mol) and 1A (−7.748 kcal/mol) presenting the most advantageous scores compared to olaparib (−8.714 kcal/mol). Binding-mode assessment identified significant interactions within the PARP1 catalytic pocket, highlighting connections with TYR889, TYR896, ARG878, ASP766, SER864, and ALA880. Significantly, 4B established a strong hydrogen-bond interaction with TYR896, while 2B paired ARG878 hydrogen bonding with a TYR896 π–π interaction. All derivatives adhered to Lipinski's rule of five and exhibited a predicted bioavailability score of 0.55, although 1A and 1B showed increased lipophilicity, with 1B surpassing the Veber rotatable-bond criterion. ADMET predictions also suggested that blood–brain barrier penetration varied by compound and highlighted significant potential issues related to CYP2C19, CYP2C8, and certain CYP1A2 and CYP2C9 pathways. Together, these results pinpoint 1A and 1B as the top docking candidates, underscoring the importance of metabolic optimization and experimental confirmation before definitive PARP1 inhibitory effects can be confirmed.

Keywords: Enaminones; PARP1 inhibitors; Molecular docking; ADMET profiling; Cyclopentane derivatives; In silico evaluation.

الملخص
يمثل إنزيم بوليميراز عديد (Poly(ADP-ribose) polymerase 1) (PARP1) هدفًا علاجيًا هامًا في علاج السرطان، لا سيما في مجال إصلاح الحمض النووي (DNA). ومع ذلك، لم تُدرس مركبات الإينامينون المشتقة من السيكلوبنتان بشكلٍ كافٍ كأنماط كيميائية ترتبط بإنزيم PARP1. في هذا البحث، تم تقييم عشرة مركبات إينامينون مشتقة من السيكلوبنتان

 Copyright: © 2026 by the authors. Submitted for possible open access publication under the terms and conditions of the Creative Commons Attribution (CC BY) license (https://creativecommons.org/licenses/by/4.0/).

(A–5A1 وB–5B1) تم تطويرها سابقًا، وذلك من خلال محاكاة الارتباط الجزيئي القائمة على البنية مع النطاق التحفيزي لإنزيم PARP1 البشري (PDB ID: 7KK4)، تلاها تقييمات حاسوبية شاملة لحركية الدواء، وخصائص الدواء، والسمية. تم تأكيد بروتوكول محاكاة الارتباط من خلال إعادة محاكاة ارتباط مثبط أولاباريب المتبلور معه، مما أسفر عن انحراف معياري جذري (RMSD) متوسط قدره 1.183 Å. أظهرت المشتقات المدروسة قيمًا لمؤشرات الارتباط (S-scores) تتراوح بين -6.234 و-7.972 kcal/mol، حيث حقق المركبان B1 (-7.972 kcal/mol) وA1 (-7.748 kcal/mol) أفضل النتائج مقارنةً بالأولاباريب (-8.714 kcal/mol). وكشف تقييم نمط الارتباط عن تفاعلات مهمة داخل الجيب التحفيزي لـ PARP1، مُسلطًا الضوء على الروابط مع الأحماض الأمينية TYR889 وTYR896 وARG878 وASP766 وSER864 وALA880. ومن الجدير بالذكر أن المركب B4 شكّل رابطة هيدروجينية قوية مع TYR896، بينما جمع المركب B2 بين رابطة هيدروجينية مع ARG878 وتفاعل π–π مع TYR896. التزمت جميع المشتقات بقاعدة ليبينسكي (Lipinski's rule) الخماسية، وأظهرت درجة توافر حيوي متوقعة قدرها 0.55، على الرغم من أن المركبين A1 وB1 أظهرا زيادة في محبة الدهون، حيث تجاوز المركب B1 معيار فيبر للروابط القابلة للدوران. كما أشارت تنبؤات ADMET إلى أن اختراق الحاجز الدموي الدماغي يختلف باختلاف المركب، وسلطت الضوء على مشكلات محتملة هامة تتعلق بمسارات CYP2C19 وCYP2C8 وبعض مسارات CYP1A2 وCYP2C9. تشير هذه النتائج مجتمعةً إلى أن المركبين A1 وB1 هما أفضل المرشحين للالتحام الجزيئي، مما يؤكد أهمية التحسين الأيضي والتأكيد التجريبي قبل تأكيد التأثيرات المثبطة لـ PARP1 بشكل قاطع.

الكلمات المفتاحية: إينامينونات؛ مثبطات PARP1؛ الالتحام الجزيئي؛ تحديد خصائص ADMET؛ مشتقات سيكلوبنتان؛ التقييم الحاسوبي.

1. Introduction

Enamines and their conjugated carbonyl analogs, enaminones (derived from β-dicarbonyl substrates), represent a foundational group of electron-rich organic intermediates where an amino group is attached to a carbonyl moiety via a double bond [1–3]. Functionally analogous to enols, the core reactivity and synthetic value of enamines were established through the foundational work of Mannich [4], Wittig [5], and Stork [6–9]. Because of their push–pull architecture, these systems exhibit a distinct electronic asymmetry, with the nucleophilic nitrogen donating electron density and the conjugated carbonyl group exerting an electron-withdrawing effect [2]. This unique profile enables enaminones to participate in a wide variety of synthetic transformations, such as nucleophilic and electrophilic substitutions, cycloadditions, reductions, and photochemical processes [10–17]. Furthermore, sustainable methods like heterogeneous catalysis in line with green chemistry principles have significantly streamlined their synthesis.[18 ,2]

Beyond their traditional utility as synthetic building blocks [1, 3, 19, 20], the enaminone scaffold plays an essential role in medicinal chemistry, largely due to its ability to engage in robust non-covalent interactions and dynamic hydrogen-bonding networks with biological macromolecules [19–39]. As a result, derivatives containing the enaminone core demonstrate a broad spectrum of pharmacological properties, including antibacterial [1, 39, 40], anti-inflammatory [39, 41], antitubercular [42], anticonvulsant and anti-epileptic [43–45], antifungal [39, 46], antiviral [39], antiparasitic [47], and antitumor or anticancer effects.[49 ,48]

Poly(ADP-ribose) polymerase 1 (PARP1) is a critical nuclear enzyme involved in DNA repair pathways, making its inhibition a key strategy in targeted cancer therapy, particularly for tumors showing deficiencies in homologous recombination. While enaminone derivatives are well-documented for their cytotoxic and antitumor properties [48, 49], their capability to act as targeted catalytic inhibitors of PARP1 remains largely unexplored. To bridge this gap, this study investigates ten previously synthesized cyclopentane-based enaminone derivatives (1A–5A and 1B–5B) using an *in silico* approach [18]. By conducting molecular docking simulations against the catalytic domain of PARP1 (PDB ID: 7KK4) [50], alongside detailed pharmacokinetic and ADMET evaluations, this work aims to clarify the binding interactions, hydrophobic networks, and drug-like properties of these scaffolds, thereby highlighting their potential as novel PARP1 inhibitors.

2. Computational detail

2.1 Ligand preparation

The initial 3D conformations of the target ligands **(1A–5A and 1B–5B, Scheme 1)** underwent structural optimization using the Energy Minimize module in MOE 2024 [51]. After assigning partial charges, energy minimization was carried out using the Amber: EHT force field alongside an implicit reaction field solvation model (R-Field 1:80). The optimization continued until convergence was achieved at an RMS gradient threshold of 0.1 kcal/mol / Å².

 Copyright: © 2026 by the authors. Submitted for possible open access publication under the terms and conditions of the Creative Commons Attribution (CC BY) license (https://creativecommons.org/licenses/by/4.0/).

2.2 Receptor preparation

The 3D crystallographic coordinates for the catalytic domain of human poly(ADP-ribose) polymerase 1 (PARP1, PDB ID: 7KK4) [52] were retrieved from from the RCSB Protein Data Bank. Before performing molecular docking, all crystallographic water molecules were stripped from the structure. The target protein was refined using the QuickPrep module in MOE 2024, which entails retaining chain sequences, neutralizing electrostatic charges, carrying out 3D protonation via Protonate3D with side-chain flips for ASN, GLN, and HIS, and adding missing hydrogen atoms. Afterward, a tethered energy minimization was applied (Strength: 10, Buffer: 0.25 Å; fixed atoms > 8.0 Å) until reaching an RMS gradient convergence criterion of 0.1 kcal/mol/Å^2.

2.3 Molecular Docking and Validation Study

Molecular docking calculations and scoring were performed using the Molecular Operating Environment software suite, MOE (Molecular Operating Environment (MOE), 2024). The crystallographic structure of the human poly(ADP-ribose) polymerase 1 (PARP1) catalytic domain (PDB entry: 7KK4) features a resolution of 1.96 Å. In computational docking, resolutions ranging between 1.5 and 2.5 Å are widely recognized as optimal for ensuring structural reliability [53 , 54]. Validation of docking protocol relies primarily on two key criteria: root-mean-square deviation (RMSD) values at or below 2.0 Å and binding free energy scores equal to or lower than -7 [55].

2.4 In Silico ADME and Toxicity Predictions

Pharmacokinetic profiling and toxicity assessments for compounds (1A_5A , 1B_5B) were conducted using integrated web-based computational platforms, including SwissADME, ADMETlab 3.0, and ProTox 3.0 (https://tox.charite.de/protox3). The canonical Simplified Molecular Input Line Entry System (SMILES) notations of the target compounds were obtained from the PubChem database and utilized as input for all predictive servers. Key ADME parameters—such as human intestinal absorption (HIA), blood-brain barrier (BBB) penetration, cytochrome P450 enzyme inhibition, and compliance with Lipinski's Rule of Five—were evaluated using SwissADME, and ADMETlab 3.0 to determine their drug-likeness potential. Furthermore, comprehensive toxicological profiles were predicted using ProTox 3.0, which integrates molecular similarity, fragment-based analysis, and machine-learning approaches across 61 predictive models to estimate various toxicity endpoints, organ toxicities, and toxicological pathways [56 , 57 , 58].

3.Results and discussion

In this study, a series of ten previously synthesized cyclopentane derivatives (**1A–5A** and **1B–5B**, **Scheme 1**) were evaluated to explore their binding interactions and inhibitory mechanisms against the PARP1 catalytic domain (PDB ID: 7KK4) using molecular docking.

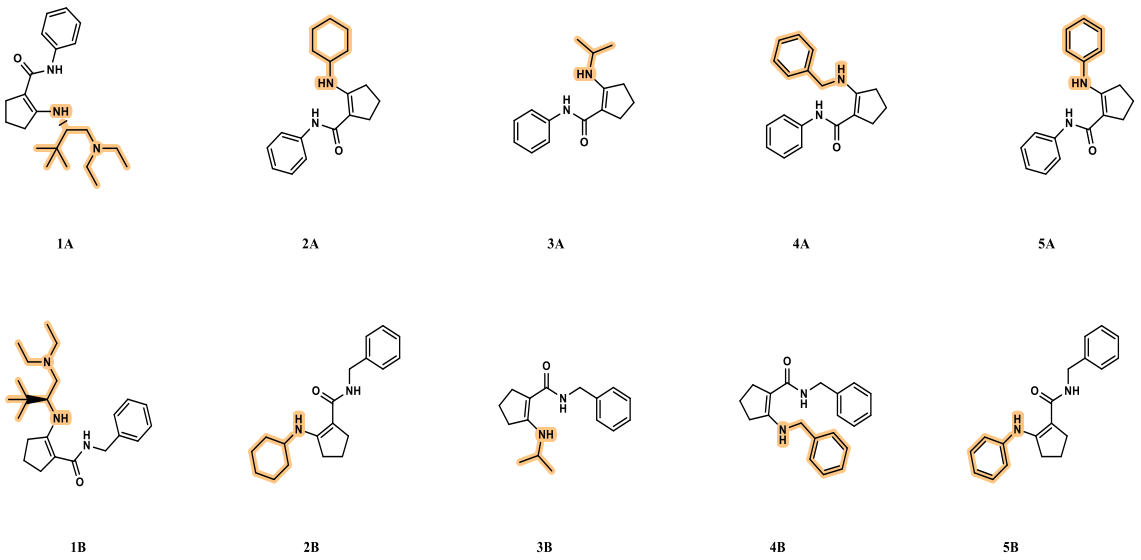

Scheme 1. Chemical structures of the studied cyclopentane derivatives (1A–5A and 1B–5B), highlighting the variable amine substituent

 Copyright: © 2026 by the authors. Submitted for possible open access publication under the terms and conditions of the Creative Commons Attribution (CC BY) license (https://creativecommons.org/licenses/by/4.0/).

3.1 Docking Protocol Validation and Binding Mode Analysis

To assess the reliability and predictive capacity of the chosen molecular docking protocol, a self-docking (re-docking) study was caried out before screening the target compounds. The co-crystallized inhibitor, Olaparib, was isolated and re-docked into the active catalytic domain of PARP1 (PDB ID: 7KK4). As depicted in Figure 3.1 , overlaying the generated docked pose (red) onto the authentic crystallographic conformation (yellow) revealed a high degree of structural alignment, achieving a Root Mean Square Deviation (RMSD) of 1.183 Å. Since this value is substantially below the universally accepted threshold of 2.0 Å It unequivocally confirms the robustness, accuracy, and reproducibility of the docking parameters in reproducing authentic binding geometries.

Figure 1. Validation of the docking protocol by re-docking Olaparib into PARP1 (PDB ID: 7KK4; RMSD = 1.183 Å)

3.2 Binding Interaction Analysis of Olaparib (Reference Lead):

The reference drug Olaparib demonstrated substantial affinity for the catalytic cavity of PARP1, yielding an S-score of -8.714 kcal/mol. Stabilization of Olaparib within the pocket relies primarily on key hydrogen bonds and hydrophobic contacts. Specifically, a prominent hydrogen bond is formed between its carbonyl oxygen (OAC 26) and the backbone nitrogen of TYR 896 (distance = 2.97 Å, E = -4.1 kcal/mol), alongside a secondary hydrogen bond with LYS 903 (distance = 3.29 Å, E = -0.7 kcal/mol). Furthermore, the aromatic rings engage in a hydrophobic π-π stacking interaction between its aromatic ring system and TYR 896 (distance = 4.04 Å).

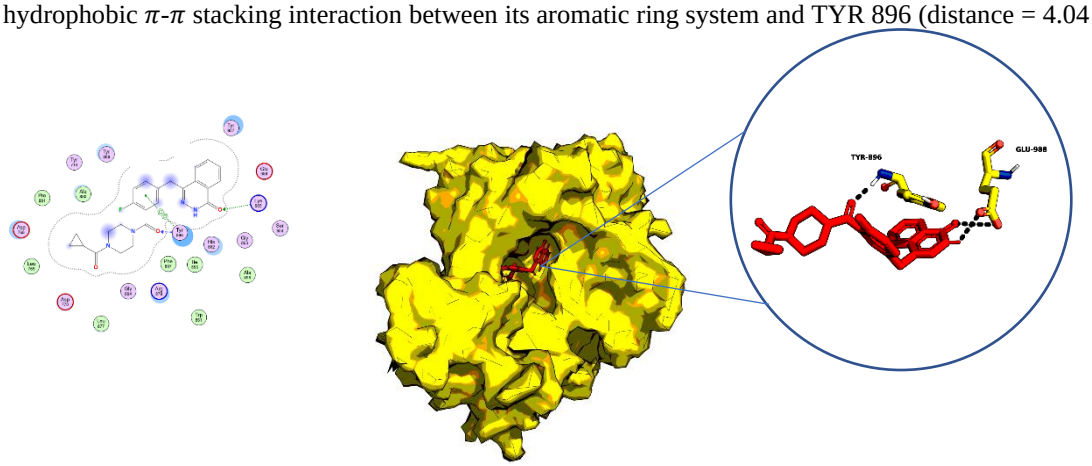

Figure 2. 2D and 3D binding interactions of the reference drug Olaparib within the catalytic active site of PARP1 (PDB ID: 7KK4)

3.3 Comparative Binding Modes of the Designed Series (1A–5A and 1B–5B):

All tested derivatives (1A–5A and 1B–5B, Scheme 1) demonstrated favorable binding energies spanning from -6.234 kcal/mol (3Å) to -7.972 kcal/mol (1B). Most Notably, compounds 1B ($S = -7.972$ kcal/mol) and **1A** ($S = -7.748$ kcal/mol) showed the strongest binding affinities, coming quite close to the performance level of Olaparib.

Detailed inspection of the binding interactions revealed that several derivatives conserved the key interactions observed in the reference drug:

- **Key H-Bonding with TYR 896 & ASP 766:** Compound **4B** exhibited a highly potent hydrogen bond with **TYR 896** (distance = 2.96 Å), yielding a remarkable interaction energy ($E = -6.4$ kcal/mol) that exceeds that of Olaparib itself. Compound **5A** established a dual-contact network involving **ARG 878** (3.42 Å) and **TYR 896** (3.08 Å, $E = -3.3$ kcal/mol). Meanwhile, derivatives **2A** and **5B** effectively engaged the acidic residue **ASP 766** through H-donor bonds at **3.03 Å** and **2.99 Å**, respectively.
- **Aromatic and Hydrophobic Networks:** π-mediated interactions played a decisive role in stabilizing the series. Compounds **1A** and **1B** predominantly relied on π-H contacts with **TYR 889**. Furthermore, compound **2B** mirrored Olaparib's binding topology by combining an H-bond to **ARG 878** (3.02 Å) with a π-π stacking interaction against **TYR 896** (4.12 Å). Additional hydrophobic contacts with **ALA 880**, **TYR 907**, and **ASN 767** provided overall structural stability across the series.

 Copyright: © 2026 by the authors. Submitted for possible open access publication under the terms and conditions of the Creative Commons Attribution (CC BY) license (https://creativecommons.org/licenses/by/4.0/).

Table 1. The results obtained from docking of Ligands with 7KK4

Ligands	S score (kcal/mol)	RMSD (Å)	Atom of compound	Atom of receptor	Involved receptor residues	Type of interaction bond	Distance (Å)	E(kcal/mol)
1A	-7.748	1.507	6-ring	CD2	TYR 889	pi-H	3.74	-0.5
2A	-6.591	1.474	N 14	OD2	ASP 766	H-donor	3.03	-4.0
3A	-6.234	0.899	N 14	NE2	HIS 862	H-donor	3.59	-1.4
4A	-6.441	1.368	O 13	OG	SER 864	H-acceptor	2.99	-1.3
5A	-6.485	1.171	N 14 O 13	O N	ARG 878 TYR 896	H-donor H-acceptor	3.42 3.08	-1.3 -3.3
1B	-7.972	1.643	C 6 6-ring	6-ring CA	TYR 889 TYR 889	H-pi pi-H	3.85 4.11	-0.6 -0.7
2B	-6.621	1.075	N 16 6-ring	O 6-ring	ARG 878 TYR 896	H-donor pi-pi	3.02 4.12	-1.1
3B	-6.744	1.289	O 13 6-ring	OG ND2	SER 864 ASN 767	H-acceptor pi-H	2.83 3.68	-2.9 -0.7
4B	-6.689	1.253	O 13 C 42 6-ring	N 6-ring CA	TYR 896 TYR 907 ALA 880	H-acceptor H-pi pi-H	2.96 4.30 3.53	-6.4 -0.5 -0.5
5B	-6.604	1.229	N 14 6-ring	OD2 CA	ASP 766 ALA 880	H-donor pi-H	2.99 3.55	-1.5 -0.5
Ref ligand	-8.714	1.183	OAC 26 OAD 52 6-ring	N CE 6-ring	TYR 896 LYS 903 TYR 896	H-acceptor H-acceptor pi-pi	2.97 3.29 4.04	-4.1 -0.7

Number Ligands	A	B
1	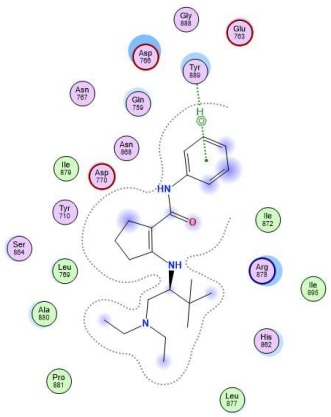	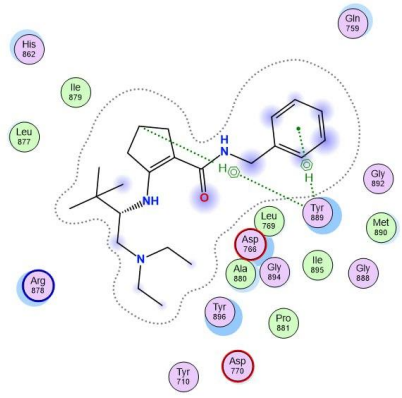

 Copyright: © 2026 by the authors. Submitted for possible open access publication under the terms and conditions of the Creative Commons Attribution (CC BY) license (https://creativecommons.org/licenses/by/4.0/).

Number Ligands	A	B
2	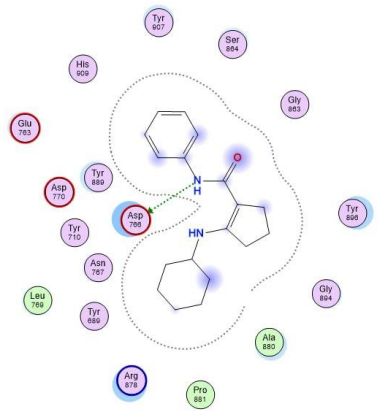	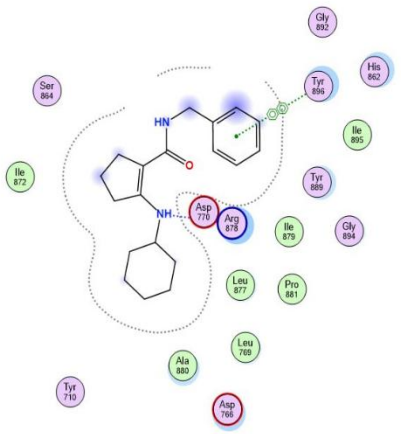
3	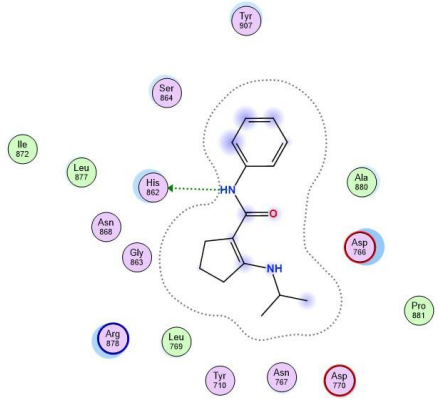	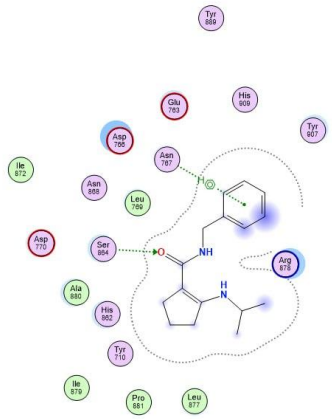
4	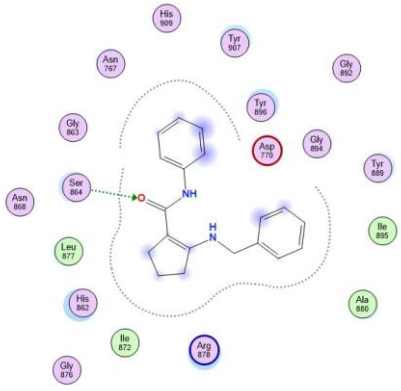	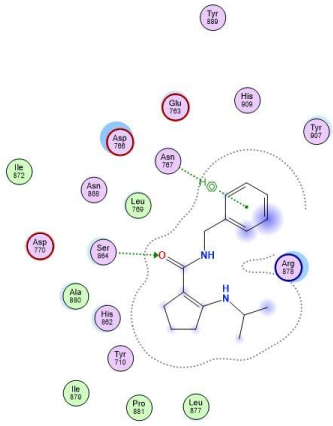

 Copyright: © 2026 by the authors. Submitted for possible open access publication under the terms and conditions of the Creative Commons Attribution (CC BY) license (https://creativecommons.org/licenses/by/4.0/).

Number Ligands	A	B
5	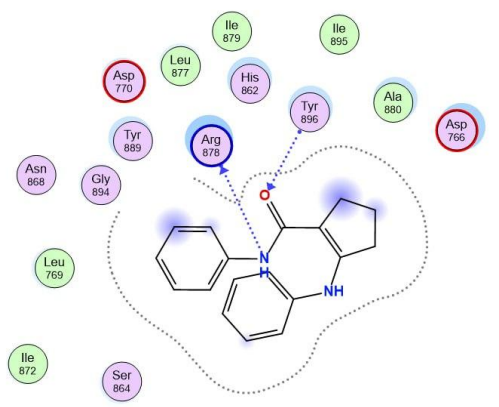	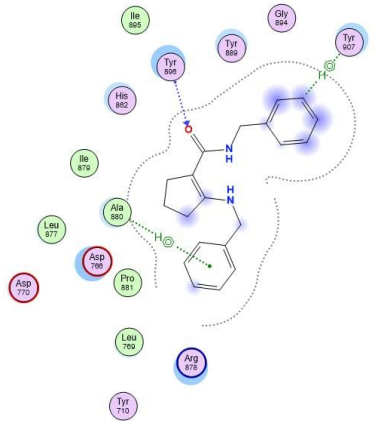

Figure 3. 2D binding interaction diagrams of the studied cyclopentane derivatives (1A–5A and 1B–5B) inside the PARP1 catalytic pocke

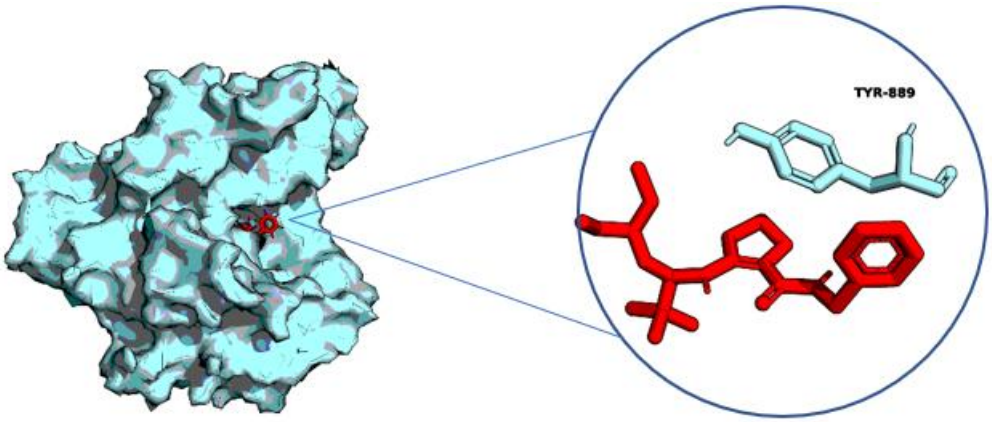

1B

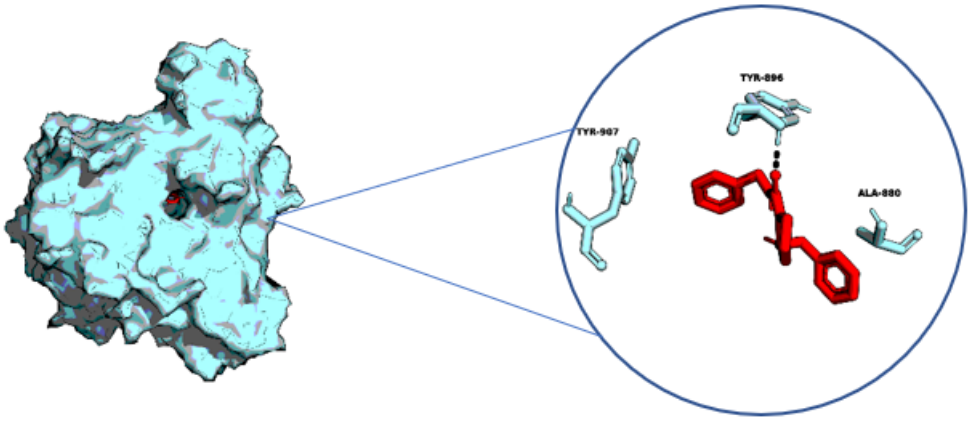

4B

Figure 4. 3D binding modes of top derivatives (1B and 4B) in the PARP1 catalytic site (PDB ID: 7KK4)

 Copyright: © 2026 by the authors. Submitted for possible open access publication under the terms and conditions of the Creative Commons Attribution (CC BY) license (https://creativecommons.org/licenses/by/4.0/).

3.4 ADME and toxicity profile analysis

3.4.1 Physicochemical and drug-likeness properties

The physicochemical and drug-like attributes of derivatives 1A–5A and 1B–5B showed overall positive profiles. Molecular weights varied between 244.33 and 371.56 g/mol, remaining well below the conventional 500 g/mol limit linked to Lipinski's rule of five. The count of heavy atoms ranged from 18 to 27, while the proportion of sp^3-hybridized carbons (Fcp^3) ranged from 0.17 to 0.61. Significantly, the B-series derivatives consistently displayed marginally elevated Fcp^3 values compared to their A-series counterparts, indicating enhanced three-dimensional character and molecular saturation.

The count of rotatable bonds varied between 5 and 11, suggesting moderate to acceptable conformational flexibility. Compound 1B showed the greatest quantity of rotatable bonds (11), leading to one violation of the Veber rule, while the other derivatives adhered to the Veber guideline. All compounds included solely 1–2 hydrogen-bond acceptors and two hydrogen-bond donors, with fairly low topological polar surface area (TPSA) values ranging from 41.13 to 44.37 $Å^2$. These values indicate that high molecular polarity is probably not a significant barrier to passive membrane permeability.

All ten derivatives met Lipinski's criteria without any violations and were in accordance with the Ghose and Egan filters. The majority of derivatives also fulfilled the Muegge criteria; however, compounds 1A and 1B showed one Muegge violation associated with XLOGP3 > 5, suggesting relatively higher lipophilicity. Compound 1B additionally violated the Veber criterion because of its high number of rotatable bonds. Nevertheless, all derivatives displayed a predicted bioavailability score of 0.55, supporting an overall favorable drug-like profile. These results suggest that structural changes between the A and B series did not substantially compromise classical drug-likeness characteristics.

3.4.2 Absorption and distribution parameters

The anticipated absorption and distribution parameters indicated relatively consistent intestinal permeability among the examined derivatives. Caco-2 permeability values ranged from −4.99445 to −4.61503, with compounds 1B and 2B demonstrating the highest numerical values (−4.64655 and −4.61503, respectively). MDCK permeability estimations were also similar across the derivatives, varying roughly between 1.09×10^{-5} to 2.50×10^{-5}, suggesting broadly similar membrane transport behavior within the series.

The probabilities of P-glycoprotein substrates were quite low for the majority of derivatives, which may suggest a reduced susceptibility to efflux mediated by P-gp. Compound 3A stood out as a significant exception, exhibiting a notably higher predicted P-gp substrate probability of 0.553 in contrast to the other compounds. This variation might suggest that 3A could be more vulnerable to transporter-mediated removal, likely decreasing intracellular exposure compared to structurally similar derivatives.

The anticipated volume of distribution (VDss) showed increased variability, ranging from 0.481 for 5B to 2.524 for 1A. Consequently, compound 1A demonstrated the highest expected distribution potential, succeeded by 3A and 1B, while compounds 2B–5B typically displayed reduced VDss values. This variation implies that the structural changes differentiating the two series could affect tissue distribution, even though their physicochemical properties are similar.

Significant distinctions were also noted in the anticipated blood–brain barrier (BBB) profiles. Compounds 1A and 1B showed significantly low BBB probabilities of 0.00397 and 0.01197, respectively, while compounds 4A, 2B, 3B, 4B, and 5B demonstrated considerably higher predicted values of 0.899, 0.863, 0.964, 0.974, and 0.955, respectively. Consequently, aside from 1B, the subsequent members of the B series exhibited a marked inclination for anticipated BBB permeability. Depending on the specific therapeutic application, this behavior can be beneficial for central nervous system targets or pose a potential risk for compounds aimed at peripheral action.

Predictions of transporter interactions also suggested significant structural reliance. The interaction probabilities of OATP1B1 were especially high for 1A and 1B, both nearing 1.0, and stayed relatively high for numerous A-series derivatives. In comparison, compounds 2B–5B demonstrated significantly reduced probabilities for OATP1B1. Interactions with OATP1B3 were notably stronger, with multiple derivatives demonstrating probabilities exceeding 0.8. Overall, these results indicate that the disposition mediated by hepatic transporters might have varying influences on the pharmacokinetic profiles of each derivative.

3.4.3 Metabolic stability profile

Predictions for cytochrome P450 showed significant variations in metabolic vulnerability among the created derivatives. Compounds 3A, 4A, and 5A showed remarkably high projected CYP1A2 inhibition probabilities (>0.99), while 1B and 2B revealed significantly lower figures of about 0.060 and 0.015, respectively. The B-series derivatives 3B–5B displayed consistently high probabilities of CYP1A2 inhibition (0.884–0.967), suggesting that the influence is primarily linked to specific structural substitutions rather than solely on the A/B scaffold.

 Copyright: © 2026 by the authors. Submitted for possible open access publication under the terms and conditions of the Creative Commons Attribution (CC BY) license (https://creativecommons.org/licenses/by/4.0/).

CYP2C19 inhibition indicated a more significant anticipated risk, as most derivatives demonstrated elevated probabilities. Specifically, compounds 2A–5A and 2B–5B demonstrated values typically greater than 0.94. A comparable pattern was noted for CYP2C8, with numerous derivatives, especially 3A, 4A, 2B, and 3B–5B, exhibiting probabilities nearing one. Inhibition of CYP2C9 was similarly significant for 4A, 5A, and 3B–5B. These findings indicate that multiple derivatives may have the potential for CYP-mediated drug–drug interactions and thus require experimental enzyme-inhibition investigations.

CYP2D6 forecasts showed notable variability. Compounds 1A, 4A, 1B, 3B, and 4B demonstrated comparatively low probabilities, while 2A and 5B displayed elevated values of about 0.824 and 0.765, respectively. The behavior of CYP3A4 substrates also showed significant variation. Compounds 1A and 1B exhibited extremely high substrate probabilities of around 0.996 and 0.985, whereas 4B also displayed a significant value of 0.955. Conversely, multiple other derivatives showed relatively low probabilities of being CYP3A4 substrates. All derivatives showed extremely low probabilities as CYP2B6 substrates, indicating that metabolism via this route might be quite restricted.

In summary, the CYP profile suggests that advantageous physicochemical drug-likeness does not automatically correspond to a similarly advantageous metabolic profile. The elevated anticipated inhibition probabilities for CYP2C19, CYP2C8, and, for specific derivatives, CYP1A2 and CYP2C9 indicate possible metabolic risks that must be taken into account during subsequent lead optimization.

3.4.4 Excretion and pharmacokinetic parameters

Estimated plasma clearance values varied from about 4.38 to 7.65 among the derivatives. Compounds 1A and 1B demonstrated the highest anticipated clearance values of 7.37 and 7.65, respectively, while 4A presented the lowest value of around 4.38. The other compounds showed moderate clearance profiles.

Estimated half-life values varied between roughly 0.296 and 0.693. Compound 5A showed the highest estimated T1/2 value (0.693), followed by 5B (0.555), while 2B demonstrated the lowest value (0.296). The shorter anticipated half-lives noted for various derivatives, especially 1A, 2A, 1B, and 2B, might suggest a more rapid systemic clearance. Yet, these computational estimates need to be regarded as comparative pharmacokinetic markers instead of direct replacements for experimentally obtained clearance and plasma half-life.

3.4.5 Toxicity risk assessment

ProTox 3.0 predictions showed significant variations in the toxicity profiles of the studied derivatives. Estimated LD50 values varied between 578 and 24,000 mg/kg, with compounds 4A and 5B presenting the highest LD50 values and placed in toxicity class 6, while 2B showed the lowest LD50 (578 mg/kg) and was categorized as class 4.

The probabilities of organ-specific toxicity were moderate to fairly high throughout the series, especially for hepatotoxicity (0.68–0.81), while neurotoxicity, nephrotoxicity, respiratory toxicity, and cardiotoxicity exhibited relatively narrower ranges. Significantly, 1A and 1B showed comparatively high anticipated hepatotoxicity, respiratory toxicity, and cardiotoxicity, even with their positive docking results. These results suggest a possible compromise between anticipated PARP1 binding strength and toxicity risk. Consequently, the ProTox findings must be viewed as initial computational markers, and experimental toxicological confirmation is necessary prior to additional lead advancement.

 Copyright: © 2026 by the authors. Submitted for possible open access publication under the terms and conditions of the Creative Commons Attribution (CC BY) license (https://creativecommons.org/licenses/by/4.0/).

Table 2. Physicochemical properties and drug-likeness for Cyclopentane (1A-5A), (1B-5B)

Ligands	Physiological properties							Drug likeness properties					
	Molecular weight	Num. heavy atoms	Fraction Csp3	Num. rotatable bonds	Num. H-bond acceptors	Num. H-bond donors	TPSA	Lipinski	Ghose	Veber	Egan	Muegge	Bio. score
1A	357.53 g/mol	26	0.59	10	2	2	44.37 Å²	Yes; 0 violation	Yes	Yes	Yes	No; 1 violation: XLOGP3>5	0.55
2A	284.40 g/mol	21	0.50	5	1	2	41.13 Å²	Yes; 0 violation	Yes	Yes	Yes	Yes	0.55
3A	244.33 g/mol	18	0.40	5	1	2	41.13 Å²	Yes; 0 violation	Yes	Yes	Yes	Yes	0.55
4A	292.37 g/mol	22	0.21	6	1	2	41.13 Å²	Yes; 0 violation	Yes	Yes	Yes	Yes	0.55
5A	278.35 g/mol	21	0.17	5	1	2	41.13 Å²	Yes; 0 violation	Yes	Yes	Yes	Yes	0.55
1B	371.56 g/mol	27	0.61	11	2	2	44.37 Å²	Yes; 0 violation	Yes	No; 1 violation: Rotors> 10	Yes	No; 1 violation: XLOGP3>5	0.55
2B	298.42 g/mol	22	0.53	6	1	2	41.13 Å²	Yes; 0 violation	Yes	Yes	Yes	Yes	0.55
3B	258.36 g/mol	19	0.44	6	1	2	41.13 Å²	Yes; 0 violation	Yes	Yes	Yes	Yes	0.55
4B	306.40 g/mol	23	0.25	7	1	2	41.13 Å²	Yes; 0 violation	Yes	Yes	Yes	Yes	0.55
5B	292.37 g/mol	22	0.21	6	1	2	41.13 Å²	Yes; 0 violation	Yes	Yes	Yes	Yes	0.55

Table 3. In silico ADMET profiling of Cyclopentane (1A-5A), (1B-5B) comprehensive pharmacokinetic and toxicity predictions

Entry	1A	2A	3A	4A	5A	1B	2B	3B	4B	5B
Absorption/distribution										
CaCo2	-4.78336	-4.76554	-4.82609	-4.95574	-4.99445	-4.64655	-4.61503	-4.68345	-4.78397	-4.92302
MDCK	1.38E-05	2.5E-05	2.49E-05	2.25E-05	2.31E-05	1.09E-05	1.73E-05	1.68E-05	1.56E-05	2.19E-05
pgb substrate	0.004613	0.026355	0.552576	0.020343	0.004411	2.79E-05	0.000257	0.004374	0.000152	8.18E-05
VDss	2.524393	1.11086	1.535226	0.735846	0.921039	1.460593	0.53177	0.717095	0.506445	0.480586
BBB	0.003966	0.506542	0.638656	0.898552	0.551783	0.011966	0.863393	0.963607	0.97354	0.954561
OATP1B1	0.99999	0.70649582	0.8538091	0.4619	0.8006296	0.999885	0.12872	0.238908	0.155662	0.1602067
OATP1B3	0.999977	0.948852	0.8301875	0.945383	0.9887323	0.999878	0.732943	0.535075	0.848461	0.839272
Metabolism										
CYP1A2-inh	0.424425125	0.310575455	0.995141745	0.991870046	0.998221576	0.059978724	0.01484899	0.966817975	0.93494761	0.883959174
CYP2C19-inh	0.416017711	0.992111444	0.944087029	0.965538144	0.992498934	0.859130442	0.995675862	0.999566495	0.999486208	0.999471724
CYP2C9-inh	0.290353805	0.33468843	0.620627463	0.942156374	0.997663379	0.699569404	0.61020261	0.997427404	0.999030828	0.999576151
CYP2D6-inh	0.140706927	0.824160814	0.319170147	0.159809008	0.570072234	0.067529216	0.48735252	0.135453954	0.099946432	0.764748156
CYP3A4-sub	0.995821834	0.009966764	0.190069124	0.503114343	0.132808253	0.984841168	0.053581227	0.026422402	0.955240071	0.035208292
CYP2B6-sub	6.49423E-12	4.52824E-08	0.000884561	1.40434E-05	9.05065E-08	1.90596E-09	3.5357E-05	0.0040936	0.009115432	0.000809655
CYP2C8-inh	0.280602664	0.944843948	0.993702829	0.972266018	0.828145683	0.895752728	0.974216282	0.999979377	0.995703995	0.999152422
Excretion										
cl-plasma	7.372653	4.711909	5.524858	4.382347	4.427265	7.646084	5.372961	6.085657	5.063097	5.14415
T1/2	0.37754	0.366591	0.446212	0.492513	0.693262	0.350912	0.295809	0.383717	0.417221	0.554641

 Copyright: © 2026 by the authors. Submitted for possible open access publication under the terms and conditions of the Creative Commons Attribution (CC BY) license (https://creativecommons.org/licenses/by/4.0/).

Organ toxicity prediction										
Predicted LD50/	2000mg/kg	2000mg/kg	6000mg/kg	24000mg/kg	6000mg/kg	1200mg/kg	578mg/kg	1200mg/kg	1200mg/kg	24000mg/kg
Predicted Toxicity Class	4	4	6	6	6	4	4	4	4	6
Hepatotoxicity	0.81	0.75	0.76	0.70	0.68	0.81	0.75	0.78	0.76	0.70
Neurotoxicity-	0.55	0.65	0.57	0.65	0.68	0.55	0.63	0.55	0.66	0.65
Nephrotoxicity-	0.64	0.63	0.63	0.59	0.64	0.62	0.58	0.59	0.59	0.59
Respiratory toxicity	0.80	0.50	0.56	0.64	0.50	0.78	0.66	0.67	0.63	0.64
Cardiotoxicity	0.70	0.64	0.65	0.66	0.69	0.70	0.65	0.64	0.68	0.66

Ligand	Distribution of M .wt	Distribution of dose value	Multi target activity profile and toxicity
4A	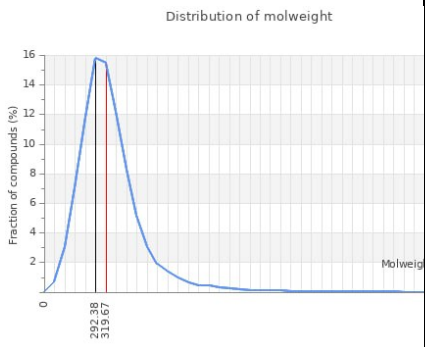	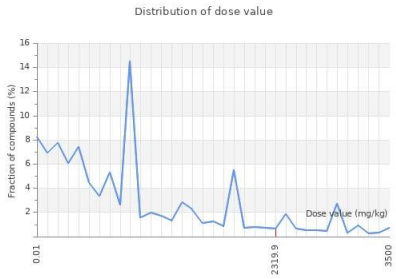	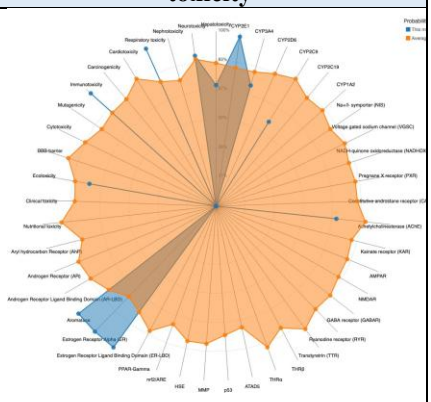
5B	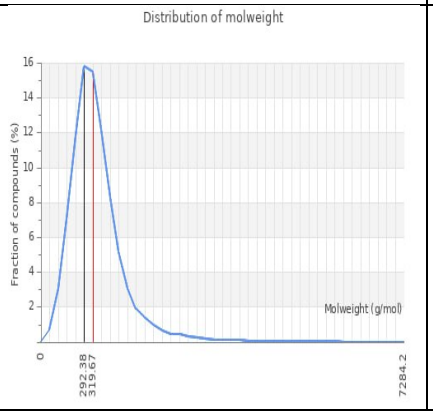	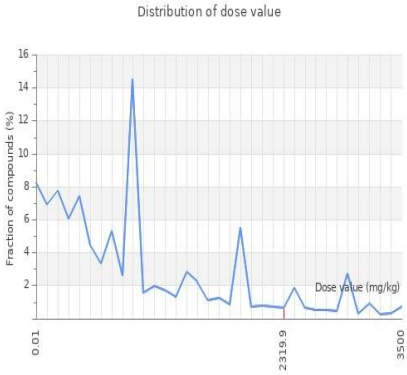	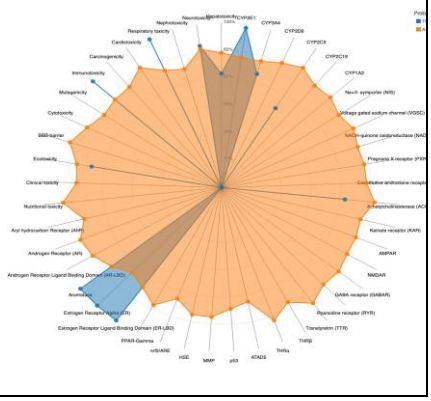

Figure 5. Distribution of toxicity prediction A4, 5B

4. Conclusion

This study offers a structure-oriented evaluation of cyclopentane-derived enaminones as possible scaffolds for PARP1 binding. The docking workflow's reliability was confirmed by the successful re-docking of olaparib into the PARP1 catalytic site, yielding an RMSD of 1.183 Å. Of the assessed derivatives, 1B and 1A showed the best docking scores, nearing that of the reference ligand, while other analogues maintained essential interactions within the catalytic pocket. Specifically, 4B formed a robust hydrogen-bond interaction with TYR896, whereas 2B, 5A, 2A, and 5B interacted with residues such as ARG878, TYR896, and ASP766, demonstrating that the cyclopentane-enaminone structure can support various binding configurations within the PARP1 active site.

Even with mostly positive physicochemical characteristics and adherence to traditional drug-likeness standards, the ADMET assessment revealed multiple drawbacks that need to be taken into account during lead optimization. Factors encompass increased lipophilicity and conformational adaptability for certain compounds,

 Copyright: © 2026 by the authors. Submitted for possible open access publication under the terms and conditions of the Creative Commons Attribution (CC BY) license (https://creativecommons.org/licenses/by/4.0/).

differing projected blood–brain barrier permeability, and high anticipated inhibition likelihoods for various cytochrome P450 isoforms, especially CYP2C19 and CYP2C8. Predictions of toxicity indicated profiles that depend on the compound, with anticipated toxicity categories varying from 4 to 6. Thus, docking affinity by itself is inadequate for certain lead selection. Compounds 1A and 1B merit precedence for experimental PARP1 inhibition investigations due to their docking outcomes, whereas 4B serves as a mechanistically pertinent analogue owing to its TYR896-centered interaction profile. Biochemical assays for enzyme inhibition, orthogonal binding analyses, cellular assessments, metabolic stability tests, and experimental evaluations of CYP and toxicity are necessary to confirm these computational predictions and assess if this scaffold can progress toward developing PARP1-targeted leads.

Compliance with ethical standards

Disclosure of conflict of interest

The authors declare that they have no conflict of interest.

References:

[1] Cindrić, M., Rubčić, M., Hrenar, T., Pisk, J., Cvijanović, D., Lovrić, J., & Vrdoljak, V. (2018). Novel enaminones as non-cytotoxic compounds with mild antibacterial activity: Synthesis and structure-activity correlations. *Journal of molecular structure*, *1154*, 636-642.

[2] Elassar, A. Z. A., & El-Khair, A. A. (2003). Recent developments in the chemistry of enaminones. *Tetrahedron*, *59*(43), 8463-8480.

[3] Ouellette RJ, Rawn JD. Organic chemistry study guide: Key concepts, problems, and solutions. Amsterdam: Elsevier; 2015.

[4] Mannich C, Davidsen H. Über einfache Enamine mit tertiär gebundenem Stickstoff. Ber Dtsch Chem Ges (A B Ser). 1936;69(9):2106-12.

[5] Wittig G, Blumenthal H. Über die Einwirkung von Ammoniak und Ammoniak-Derivaten auf o-Acetylaceto phenole. Ber Dtsch Chem Ges (A B Ser). 1927;60(5):1085-94

[6] Stork G, Terrell R, Szmuszkovicz J. A new synthesis of 2-alkyl and 2-acyl ketones. J Am Chem Soc. 1954;76(7):2029-30.

[7] Stork G, Landesman HK. A new alkylation of carbonyl compounds. II. J Am Chem Soc. 1956;78(19):5128-9

[8] Stork G, Landesman HK. A new ring enlargement sequence. J Am Chem Soc. 1956;78(19):5129-30.

[9] Stork G, Brizzolara A, Landesman H, Szmuszkovicz J, Terrell R. The enamine alkylation and acylation of carbonyl compounds. J Am Chem Soc. 1963;85(2):207-22.

[10] Nikolova, S., Kochovska, E., & Ivanov, I. (2013). Selective reduction of ortho-acylated β-enaminones of homoveratryamine and their cyclization to 1, 2, 3, 4-tetrahydroisoquinolines with β-enaminone moiety. *Synthetic Communications*, *43*(3), 326-336

[11] Al-Awadi, N. A., Ibrahim, M. R., Elnagdi, M. H., John, E., & Ibrahim, Y. A. (2012). Enaminones in a multicomponent synthesis of 4-aryldihydropyridines for potential applications in photoinduced intramolecular electron-transfer systems. *Beilstein Journal of Organic Chemistry*, *8*(1), 441-447.

[12] Kuehne ME. The arylation of enamines. J Am Chem Soc. 1962;84(5):837-47

[13] Shono T, Matsumura Y, Inoue K, Ohmizu H, Kashimura S. Electroorganic chemistry. 62. Reaction of iminium ion with nucleophile: A versatile synthesis of tetrahydroquinolines and julolidines. J Am Chem Soc. 1982;104(21):5753-7.

[14] Murahashi SI, Naotao T, Nakato T. Convenient Method for the Construction of Quinoline Skeletons from N Methylarylamines via N-(t-Butyldioxymethyl) arylamines. Synlett. 1992;1992(10):835-6

[15] Chinchilla R. In: Bäckvall JE, editor. The chemistry of enamines. New York: Wiley; 1994.

[16] Whitesell JK, Whitesell MA. Alkylation of ketones and aldehydes via their nitrogen derivatives. Synthesis. 1983;1983(7):517-36.

[17] Cook G. Enamines: synthesis, structure, and reactions. Boca Raton: CRC Press; 2017.

[18] Li Y, Wang D, Zhang L, Luo S. Redox property of enamines. J Org Chem. 2019;84(18):12071-90.

[19] Pan, L., Bi, X., & Liu, Q. (2013). Recent developments of ketene dithioacetal chemistry. *Chemical Society Reviews*, *42*(3), 1251-1286.

[20] Zhang, L., Dong, J., Xu, X., & Liu, Q. (2016). Chemistry of ketene N, S-acetals: an overview. *Chemical Reviews*, *116*(2), 287-322.

[21] Zhang Y, Qi Y, Ulrich S, Barboiu M, Ramström O. Dynamic covalent polymers for biomedical applications. Mater Chem Front. 2020;4(2):489-506

[22] Frei P, Hevey R, Ernst B. Dynamic combinatorial chemistry: a new methodology comes of age. Chem Eur J. 2019;25(1):60-73

[23] Zhang Y, Zhang Y, Ramström O. Dynamic covalent kinetic resolution. Catal Rev. 2020;62(1):66-95.

 Copyright: © 2026 by the authors. Submitted for possible open access publication under the terms and conditions of the Creative Commons Attribution (CC BY) license (https://creativecommons.org/licenses/by/4.0/).

[24] Orrillo AG, Escalante AM, Martinez-Amezaga M, Cabezudo I, Furlan RL. Molecular networks in dynamic multilevel systems. Chem Eur J. 2019;25(5):1118-27.

[25] Schaufelberger F, Timmer BJJ, Ramström O, Zhang W, Jin Y. Dynamic Covalent Chemistry: Principles, Reactions, and Applications. Weinheim: Wiley-VCH; 2017.

[26] Miljanić OŠ. Small-molecule systems chemistry. Chem. 2017;2(4):502-24.

[27] Kosikova T, Philp D. Exploring the emergence of complexity using synthetic replicators. Chem Soc Rev. 2017;46(23):7274-305.

[28] Azcune I, Odriozola I. Aromatic disulfide crosslinks in polymer systems: Self-healing, reprocessability, recyclability and more. Eur Polym J. 2016;84:147-60.

[29] Brachvogel RC, von Delius M. The dynamic covalent chemistry of esters, acetals and orthoesters. Eur J Org Chem. 2016;2016(22):3662-70.

[30] Zhang Y, Barboiu M. Constitutional Dynamic Materials—Toward Natural Selection of Function. Chem Rev. 2016;116(3):809-34.

[31] Lehn JM. Perspectives in chemistry—aspects of adaptive chemistry and materials. Angew Chem Int Ed. 2015;54(11):3276-89.

[32] Herrmann A. Dynamic combinatorial/covalent chemistry: a tool to read, generate and modulate the bioactivity of compounds and compound mixtures. Chem Soc Rev. 2014;43(6):1899-933.

[33] Hu L, Schaufelberger F, Timmer BJJ, Flos MA, Ramström O. Kirk-Othmer Encyclopedia of Chemical Technology. Hoboken: Wiley; 2014. p. 1-25.

[34] Misuraca MC, Moulin E, Ruff Y, Giuseppone N. Supramolecular polymers: From structural control to functional materials. New J Chem. 2014;38(8):3336-49.

[35] Wilson A, Gasparini G, Matile S. Functional systems with orthogonal photo- and redox inputs. Chem Soc Rev. 2014;43(5):1948-62.

[36] Jin Y, Yu C, Denman RJ, Zhang W. Recent advances in dynamic covalent chemistry. Chem Soc Rev. 2013;42(16):6634-54.

[37] Hunt RA, Otto S. Dynamic combinatorial libraries: Functional assembly in chemistry and biology. Chem Commun. 2011;47(3):847-58.

[38] Gasparini G, Dal Molin M, Prins LJ. Dynamic covalent chemistry: From discrete molecules to functional supramolecular systems. Eur J Org Chem. 2010;2010(23):2429-40.

[39] Kogan EA, Kuznetsov MT. Enamine compounds as potential bioactive agents: Recent advances. J Med Chem. 2019;62(10):4534-50.

[40] Thumar, N. J., & Patel, M. P. (2011). Synthesis, characterization, and antimicrobial evaluation of carbostyril derivatives of 1H-pyrazole. *Saudi Pharmaceutical Journal*, *19*(2), 75-83.

[41] Jyothish Kumar, L., Sarveswari, S., & Vijayakumar, V. (2018). DMFDMA catalyzed synthesis of 2-((Dimethylamino) methylene)-3, 4-dihydro-9-arylacridin-1 (2 H)-ones and their derivatives: in-vitro antifungal, antibacterial and antioxidant evaluations. *Open Chemistry*, *16*(1), 1077-1088.

[42] Bangalore, P. K., Vagolu, S. K., Bollikanda, R. K., Veeragoni, D. K., Choudante, P. C., Misra, S., ... & Kantevari, S. (2020). Usnic acid enaminone-coupled 1, 2, 3-triazoles as antibacterial and antitubercular agents. *Journal of natural products*, *83*(1), 26-35.

[43] Amaye, I. J., Heinbockel, T., Woods, J., Wang, Z., Martin-Caraballo, M., & Jackson-Ayotunde, P. (2018). 6 Hz active anticonvulsant fluorinated N-benzamide enaminones and their inhibitory neuronal activity. International Journal of Environmental Research and Public Health, 15(8), 1784.

[44] Khurana, M., Salama, N. N., Scott, K. R., Nemieboka, N. N., Bauer Jr, K. S., & Eddington, N. D. (2003). Preclinical evaluation of the pharmacokinetics, brain uptake and metabolism of E121, an antiepileptic enaminone ester, in rats. *Biopharmaceutics & drug disposition*, *24*(9), 397-407.

[45] Jackson, P. L., Hanson, C. D., Farrell, A. K., Butcher, R. J., Stables, J. P., Eddington, N. D., & Scott, K. R. (2012). Enaminones 12. An explanation of anticonvulsant activity and toxicity per Linus Pauling's clathrate hypothesis. *European journal of medicinal chemistry*, *51*, 42-51.

[46] Kumar, R., Saha, N., Purohit, P., Garg, S. K., Seth, K., Meena, V. S., ... & Chakraborti, A. K. (2019). Cyclic enaminone as new chemotype for selective cyclooxygenase-2 inhibitory, anti-inflammatory, and analgesic activities. *European journal of medicinal chemistry*, *182*, 111601.

[47] El-Shennawy, A. M., Mohamed, A. H., & Abass, M. (2007). Studies on parasitologic and haematologic activities of an enaminone derivative of 4-hydroxyquinolin-2 (1H)-one against murine schistosomiasis mansoni. *Medscape General Medicine*, *9*(1), 15.

[48] Ghorab, M. M., Ragab, F. A., Heiba, H. I., El-Gazzar, M. G., & El-Gazzar, M. G. (2018). Novel thioureido-benzenesulfonamide derivatives with enaminone linker as potent anticancer, radiosensitizers and VEGFR2 inhibitors. *Bioorganic & Medicinal Chemistry Letters*, *28*(9), 1464-1470.

[49] Riyadh, S. M. (2011). Enaminones as building blocks for the synthesis of substituted pyrazoles with antitumor and antimicrobial activities. *Molecules*, *16*(2), 1834-1853.

 Copyright: © 2026 by the authors. Submitted for possible open access publication under the terms and conditions of the Creative Commons Attribution (CC BY) license (https://creativecommons.org/licenses/by/4.0/).

[50] Ryan, K., Bolaňos, B., Smith, M., Palde, P. B., Cuenca, P. D., VanArsdale, T. L., ... & Gajiwala, K. S. (2021). Dissecting the molecular determinants of clinical PARP1 inhibitor selectivity for tankyrase1. *Journal of biological chemistry*, *296*.

[51] Molecular Operating Environment (MOE), 2024.0601; Chemical Computing Group ULC, 910-1010 Sherbrooke St. W., Montreal, QC, H3A 2R7, Canada, 2024.

[52] Becke, A. D. (1997). Density-functional thermochemistry. V. Systematic optimization of exchange-correlation functionals. *The Journal of chemical physics*, *107*(20), 8554-8560.

[53] Frisch, M. J., Trucks, G. W., Schlegel, H. B., Scuseria, G. E., Robb, M. A., Cheeseman, J. R., Scalmani, G., Barone, V., Mennucci, B., Petersson, G. A., Nakatsuji, H., Caricato, M., Li, X., Hratchian, H. P., Izmaylov, A. F., Bloin, O. J., Zheng, G., Sonnenberg, J. L., Hada, M., … Tomasi, J. (2009). Gaussian, Inc., 2009.

[54] Cavalli, A., Carloni, P., & Recanatini, M. (2006). Target-related applications of first principles quantum chemical methods in drug design. *Chemical reviews*, *106*(9), 3497-3519.

[55] Domingo, L. R., Ríos-Gutiérrez, M., & Pérez, P. (2016). Applications of the conceptual density functional theory indices to organic chemistry reactivity. *Molecules*, *21*(6), 748.

[56] lichielin O, Zoete V. SwissADME: A free web tool to evaluate pharmacokinetics, drug-likeness and medicinal chemistry friendliness of small molecules. Sci Rep. (http://www.swissadme.ch 2017;7:42717.

[57] Fu L, Shi S, Yi J, et al. ADMETlab 3.0: An updated comprehensive online ADMET prediction platform. Nucleic Acids Res. 2024;52:W422–W431.

[58] Banerjee P, Kemmler E, Dunkel M, Preissner R. ProTox 3.0: A0 (https://tox.charite.de/protox3). webserver for the prediction of toxicity of chemicals. Nucleic Acids Res. 2024;52:W513–W520.

Disclaimer/Publisher's Note: The statements, opinions, and data contained in all publications are solely those of the individual author(s) and contributor(s) and not of **AJAPAS** and/or the editor(s). **AJAPAS** and/or the editor(s) disclaim responsibility for any injury to people or property resulting from any ideas, methods, instructions, or products referred to in the content.

 Copyright: © 2026 by the authors. Submitted for possible open access publication under the terms and conditions of the Creative Commons Attribution (CC BY) license (https://creativecommons.org/licenses/by/4.0/).